Electronic Supplementary Material (ESI) for Physical Chemistry Chemical Physics.

First and second deprotonation of H_2SO_4 on wet hydroxylated (0001) α-quartz: Electronic Supplementary Information (ESI)

Garold Murdachaew,[*,†] Marie-Pierre Gaigeot,[‡,¶] Lauri Halonen,[†] and R. Benny Gerber[†,§,‖]

Laboratory of Physical Chemistry, Department of Chemistry, University of Helsinki, P.O. Box 55, FI-00014 Helsinki, Finland, LAMBE, CNRS UMR 8587, Université d'Evry val d'Essonne, Boulevard François Mitterrand, Bâtiment Maupertuis, 91025 Evry, France, Institut Universitaire de France, 103 Boulevard Saint-Michel, 75005 Paris, France, Institute of Chemistry and the Fritz Haber Research Center, The Hebrew University, 91904 Jerusalem, Israel, and Department of Chemistry, University of California, Irvine, California 92697, United States

E-mail: garold.murdachaew@helsinki.fi

[*]To whom correspondence should be addressed

[†]Laboratory of Physical Chemistry, Department of Chemistry, University of Helsinki, P.O. Box 55, FI-00014 Helsinki, Finland

[‡]LAMBE, CNRS UMR 8587, Université d'Evry val d'Essonne, Boulevard François Mitterrand, Bâtiment Maupertuis, 91025 Evry, France

[¶]Institut Universitaire de France, 103 Boulevard Saint-Michel, 75005 Paris, France

[§]Institute of Chemistry and the Fritz Haber Research Center, The Hebrew University, 91904 Jerusalem, Israel

[‖]Department of Chemistry, University of California, Irvine, California 92697, United States

August 28, 2014

1 Isomeric water monolayers on hydroxylated (0001) α-quartz

Figure S1 shows the three possible H-down monolayer water structures differing by an overall 120° rotation and their energies. We find that the energies of the three structures differ by less than 1 kcal/mol, with our structure (Figure S1(a)) used here and in ref.[1] being lowest in energy.

2 Validation of theory level

We confirmed that the level of theory used for the majority of the calculations, BLYP-D2/DZVP, correctly recovered the interior and surface structure of hydroxylated (0001) α-quartz without and with the physisorbed water layer, as well as the adsorption energy of the water layer. This is shown in Figure S2 and Figure S3, respectively, and in the corresponding tables, Table S1 and Table S2, respectively.

In Table S1, it is seen that the experimental interior Si-O distance and O-Si-O angle of dry α-quartz are both well recovered by BLYP-D2 with both the DZVP and TZV2P basis sets. Comparing to Table S2, it is seen that these parameters barely change upon adsorption of the water layer. This demonstrates that our quartz layer is thick enough so that the interior structure is maintained despite surface hydroxylation or additional water physisorption.

The importance of the dispersion correction in improving the water layer-surface separation and the adsorption energy per water molecule (E_{ads}) is seen in Table S2 (compare, e.g., the BLYP/DZVP and BLYP-D2/DZVP values). E_{ads} obtained with the smaller basis set DZVP is about 15% more negative than that obtained with TZV2P (note we have not corrected for the basis set superposition error). However, given the good agreement in geometries and therefore energy gradients, the smaller basis set performs well for the dynamics. Furthermore, as shown in the main text, we observed similar behavior for both basis sets for the interaction of sulfuric acid with the wet quartz surface and also of its dissociation mechanisms and time scale. Thus we conclude that

use of the DZVP basis set for the majority of the calculations is an excellent compromise between accuracy and efficiency.

A *k*-point expansion is not implemented in CP2K. Thus, to test the validity of our setup and Γ-point only calculations with respect to *k*-point convergence, two checks were performed.

Firstly, we compared the water on quartz adsorption energy obtained in the literature calculations[2,3] of wet hydroxylated (0001) α-quartz using the DFT PW91 functional (with a plane-wave basis set; calculation converged with regard to a *k*-point expansion). Since CP2K does not implement PW91, PBE was used (without the dispersion correction but with the TZV2P basis set to more closely model the plane-wave calculation). The value obtained for E_{ads} was very close to that in refs.[2,3] (CP2K with original system size and PBE/TZV2P, -15.77 kcal/mol; VASP calculation using PW91 with a plane-wave basis set, converged with respect to a *k*-point expansion, -15.0 kcal/mol and -15.2 kcal/mol obtained in refs.[2,3]). (Note also that the geometry obtained with PBE was close to that obtained with BLYP, which shows that the structure is relatively insensitive to the DFT functional used.)

As a second test to confirm the *k*-point convergence of our initial system size, we considered the system with the surface doubled in both in-plane dimensions. The calculations for this larger system (performed with BLYP-D2/DZVP) resulted in a geometry (not shown here) nearly identical to that of the original system. Finally, as shown in Table S2, the adsorption energies per physisorbed water molecule E_{ads} were also nearly the same (original system, -20.34 kcal/mol; large, doubled system, -20.60 kcal/mol).

This validates our use of the initial system size, calculated at the Γ-point implemented in CP2K, for the majority of the calculations.

3 Trajectory details

The initial conditions for the trajectories were developed as follows. Starting with the small system and the DZVP basis set, we calculated two trajectories which differed only in the initial lateral

position and orientation of the sulfuric acid molecule relative to the surface. The acid was initially placed approximately 3.5 Å above the water layer and allowed to fall in NVE simulations at 250 K unto the equilibrated wet quartz surface. The initial H_2SO_4 rotamer was *trans*, which is lowest in energy (see ref.[4] for a discussion H_2SO_4 rotamers). In some cases, the act of falling toward the surface and interacting with the surface prior to possible deprotonation caused the acid to cycle through its rotamer states, in a few cases ending up in the *cis* state, leading to a double H-bond donor bonding configuration, an unfavored situation for deprotonation. Trajectory 1 (acid is still a *trans* rotamer upon interacting with the surface) resulted in dissociation while Trajectory 2 (acid has become a *cis* rotamer) did not. The starting configurations of the acid in Trajectories 1 and 2 were used in the runs with the larger basis set (Trajectories 3 and 4), the Large system (Trajectories 5 and 6), and at the higher temperatures (Trajectories 18 and 19; 20 and 21; and 22 and 23). This use of nearly identical starting points allowed a better understanding of, e.g., the effect on deprotonation mechanisms and time scales due to an increase in temperature (or a change in basis set) and allowed us to sidestep extensive sampling at, for example, each temperature.

It is noteworthy that the deprotonation mechanisms and time scale in the Large system were similar to those in the Small system. We can compare, e.g., in Table S3, Trajectory 5, Large system, deprotonation time of 0.49 ps, with 5 H-bonds; to Trajectory 17, Small system, deprotonation time of 0.38 ps, with 4 H-bonds. In both trajectories, a similar process of further proton migration was then observed, forming the SSIP state, etc. Thus, the possible acid coverage effect, especially the electrostatic interaction between the replica ions in neighboring PBC cells after the initial ionization (the smallest separation between replicas is just our smallest PBC dimension, 8.504 Å), did not effect these mechanisms and time scales. This was true for the coverages we have considered. Presumably, if the acid coverages had been doubled (by, for example, reducing in half one of the surface dimensions in our Small cell), an effect due to the electrostatic interaction would be observed. However, we have not considered a larger acid coverage since it is not atmospherically relevant.

To further sample the possible outcomes at 250 K, additional trajectories with the Small system

and the DZVP basis set were run. They differed in the initial orientation, lateral position, and for some, the initial height of the H_2SO_4 molecule above the surface (thereby allowing for a steering effect of the surface). We observed the acid impacting on both types of water molecules (H-flat water molecules, WI; or H-down water molecules, WII), in different orientations and conformations, and in different H-bonding environments. The majority of the trajectories were calculated at 250 K. Deprotonation was favored, with 65% of all trajectories observed to deprotonate. Most deprotonations occurred within 1 ps. In six cases dissociation was not observed within the 5–10 ps duration of the trajectory. Three of the undissociated cases corresponded to the acid in a *cis* or *cis*-like conformation donating both its H-bonds to the surface waters simultaneously, an unfavorable situation since a free acid OH is necessary for the other proton to dissociate. In the other three cases, there was insufficient solvation of the oxygens of H_2SO_4 by water hydrogens (cluster studies suggest at least three H-bonds are required). Details can be found in Table S3.

4 Deprotonation mechanisms (300 K)

See Figure S4 and Figure S5. Note that these typical deprotonation mechanisms at 300 K are similar to those at 250 K.

5 Example of a proton wire (250 K)

See Figure S6.

6 Arrhenius behavior of deprotonation rate

Figure S7 displays an Arrhenius plot of the deprotonation rate as a function of temperature. The data are from Table S3 and show the average temperatures and the estimated average dissociation times for Trajectories 1, 18, 20, and 22. For the latter three higher trajectories/temperatures, extensive sampling was not performed but the use of nearly identical starting points (see Section 3) and

the observation of similar deprotonation mechanisms allowed use of scaling.

The expense of *ab initio* molecular dynamics precluded performing simulations at a larger number of temperatures. The sparsity of the data allows only the tentative observation that the deprotonation rate appears to display an Arrhenius behavior.

7 Disordering of the water layer as a result of proton migration (250 K)

See Figure S8 and Figure S9.

8 Comparison of spectroscopic signatures at 250 and 300 K

In Figure S10 the vibrational signatures of a typical dissociating trajectory at 300 K are compared to one at 250 K. Since the mechanisms and structures at the two temperatures are very similar, the corresponding spectra are also broadly similar, with the ionization leading to the presence of the hydronium continuum and a weak bisulfate or free OH signal at both temperatures (compare Figure S4(a) and Figure S4(d) to the very similar structures at 250 K in Figure 3(a) and Figure 3(d) in the main text).

9 Low energy configurations and bonding motifs of H_2SO_4 on wet quartz from geometry optimizations

In order to better understand the energetics, some points along the trajectories (H-bonded neutral H_2SO_4 in *cis* or *trans* rotamer configurations and dissociated H_2SO_4, CIP or SSIP) were re-optimized. The results are presented in Table S4, and in Figure S11, Figure S12, and Figure S13. It is seen that the neutral, H_2SO_4 which donates both of its hydrogen atoms to water oxygens (which requires that H_2SO_4 be in its *cis* rotamer conformation) is by far the lowest energy structure. The

lowest *trans* rotamer neutral is 5.9 kcal/mol higher in energy and the lowest energy dissociated configuration (SSIP) is 6.3 kcal/mol higher in energy. In contradiction to our results, in the work of Re et al.[5] on H_2SO_4 in water clusters it was found that the ionized clusters were lower in energy for clusters with up to 5 waters. We can rationalize our result by observing that in our case of surface adsorption, the waters are on one side of the H_2SO_4 molecule only, and thus H_2SO_4 is in a *m*icro-solvated environment in which the undissociated *cis* rotamer conformation can be lowest in energy. However, in most of our trajectories, dissociation did occur, and thus the H_2SO_4 double H-donor configuration does not seem to be favored at finite temperatures, i.e., the free energy favors dissociation, and we may conjecture that even our H_2SO_4 double H-donor trajectories will eventually dissociate if the trajectories are extended in time.

The endothermicity of H_2SO_4 deprotonation in the micro-solvated environment of a vapor-water or vapor-ice interface has been observed in the work of Hynes, Bianco, and coworkers,[6–8] who also observed the discrepancy between energy and free energy and the importance and critical effect of temperature on H_2SO_4 deprotonation by computational modeling of H_2SO_4 embedded at the liquid-vapor interface.[7] They determined that at the interface, the likelihood of deprotonation is very sensitive to both solvation and temperature.[7] Thus, while energy minimizations at 0 K are useful for examining structures and attachment energies of the acid at various sites, they should be not a guide to judging the feasibility of deprotonation at finite temperatures. For that, our molecular dynamics simulations are a more reliable measure.

References

(1) Murdachaew, G.; Gaigeot, M.-P.; Halonen, L.; Gerber, R. B. Dissociation of HCl into Ions on Wet Hydroxylated (0001) α-Quartz. *J. Phys. Chem. Lett.* **2013**, *4*, 3500–3507.

(2) Yang, J.; Wang, E. G. Water adsorption on hydroxylated α-quartz (0001) surfaces: From monomer to flat bilayer. *Phys. Rev. B* **2006**, *73*, 035406.

(3) Chen, Y.-W.; Chu, I.-H.; Wang, Y.; Cheng, H.-P. Water thin film-silica interaction on α-quartz (0001) surfaces. *Phys. Rev. B* **2011**, *84*, 155444.

(4) Havey, D. K.; Feierabend, K. J.; Vaida, V. *Ab initio* study of H_2SO_4 rotamers. *J. Mol. Struct.: THEOCHEM* **2004**, *680*, 243–247.

(5) Re, S.; Osamura, Y.; Morokuma, K. Coexistence of Neutral and Ion-Pair Clusters of Hydrated Sulfuric Acid $H_2SO_4(H_2O)_n$ (n = 1–5). A Molecular Orbital Study. *J. Phys. Chem. A* **1999**, *103*, 3535–3547.

(6) Bianco, R.; Hynes, J. T. A theoretical study of the $H_2SO_4 + H_2O \rightarrow HSO_4^- + H_3O^+$ reaction at the surface of aqueous aerosols. *Theor. Chem. Acc.* **2004**, *111*, 182–187.

(7) Bianco, R.; Wang, S.; Hynes, J. T. Theoretical Study of the First Acid Dissociation of H_2SO_4 at a Model Aqueous Surface. *J. Phys. Chem. B* **2005**, *109*, 21313–21321.

(8) Bianco, R.; Hynes, J. T. Heterogeneous Reactions Important in Atmospheric Ozone Depletion: A Theoretical Perspective. *Acc. Chem. Res.* **2006**, *39*, 159–165.

(9) Deer, W. A., Howie, R. A., Zussman, J., Eds. *Introduction to the Rock-Forming Minerals*; Mineralogical Society, 1992.

(a) This work

E_{rel} = 0.00 (0.00)
E_b = -20.34 (-17.27)

(b) Each water molecule rotated clockwise about z-axis by 120°
E_{rel} = 0.49 (0.58)
E_b = -20.28 (-17.19)

(c) Each water molecule rotated clockwise about z-axis by 240°
E_{rel} = 0.67 (0.38)
E_b = -20.26 (-17.22)

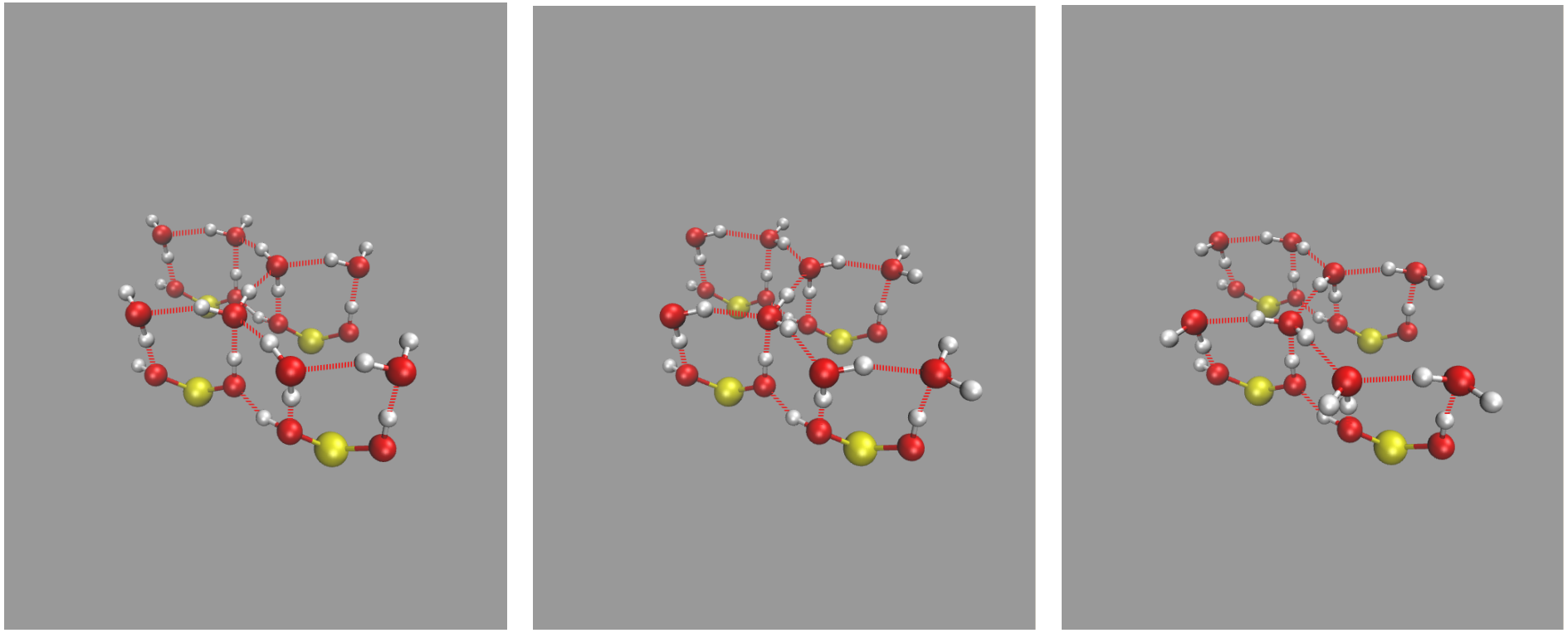

Figure S1: The three geometry-optimized water adlayer isomer structures (perspective view; silanol top layer only shown; sulfur, orange; oxygen, red; hydrogen, white; silicon, yellow) and relative energies E_{rel} and water binding energies E_b (per water monomer on the hydroxylated (0001) α-quartz surface, relative to the optimized isolated dry hydroxylated surface and the isolated single water monomer). The structures and energies were obtained using CP2K and BLYP-D2 always with the appropriate GTH pseudopotentials and the DZVP basis set (the structures obtained using the TZV2P basis set were nearly identical; the TZV2P energies are shown in parentheses). All energies are in kcal/mol.

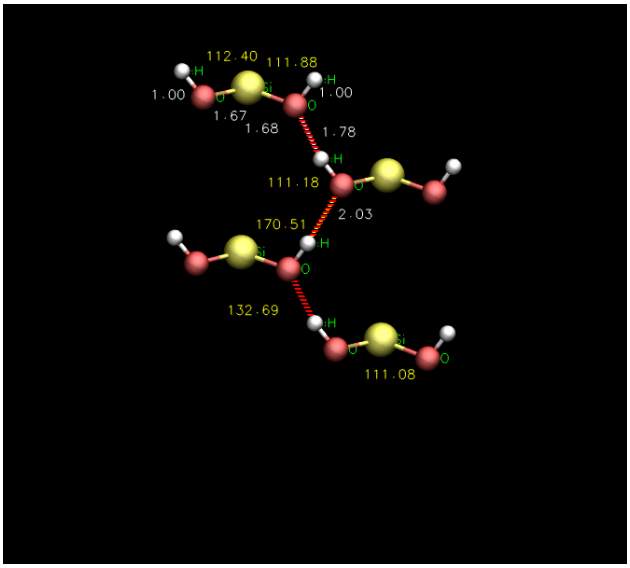

(a) Dry surface: Top view

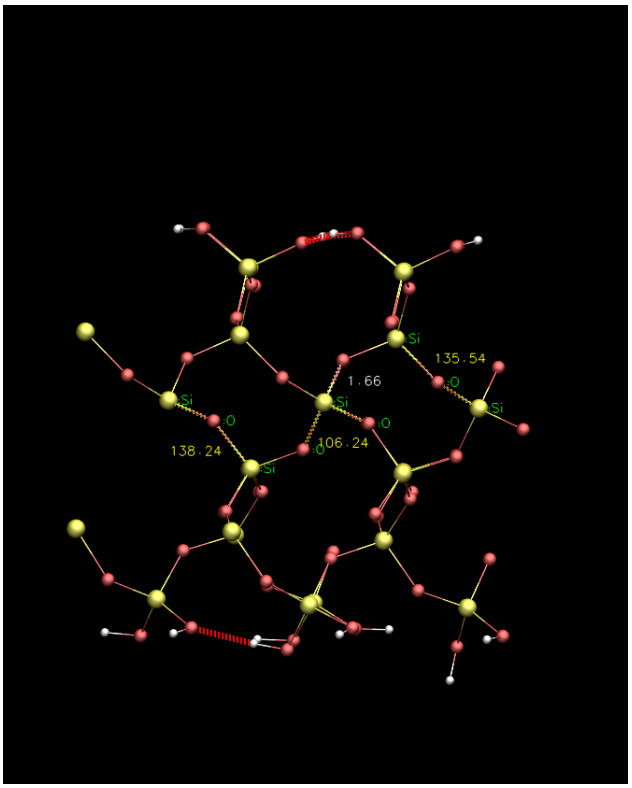

(b) Dry surface: Side view

Figure S2: Images of the optimized hydroxylated (0001) α-quartz surface and its geometrical parameters obtained using CP2K and BLYP-D2/DZVP. Dry surface (without physisorbed water): (a) top view (silanol top layer only shown) and (b) side view.

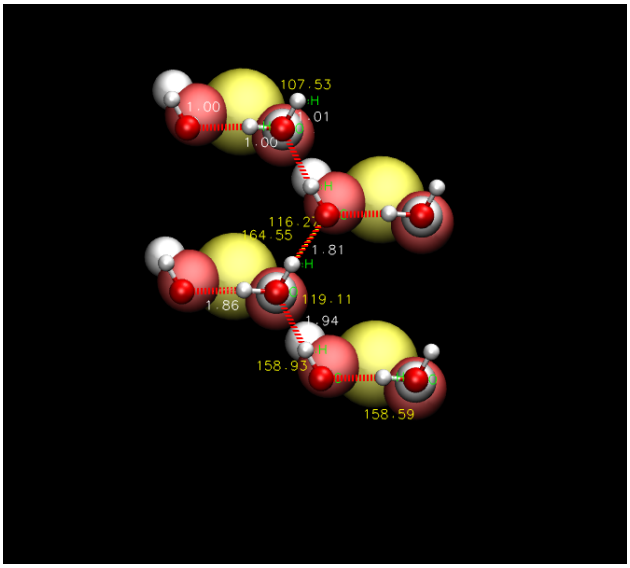

(a) Wet surface: Top view

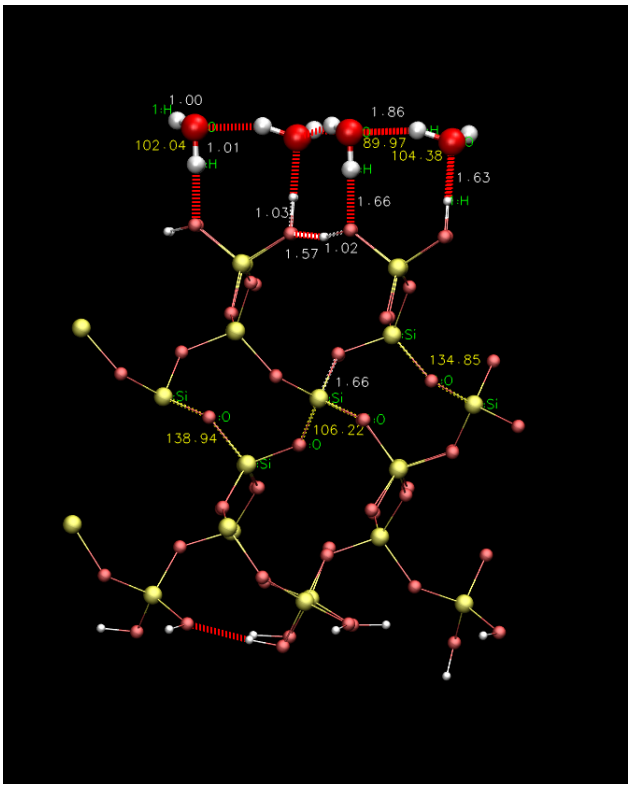

(b) Wet surface: Side view

Figure S3: Images of the optimized hydroxylated (0001) α-quartz surface and its geometrical parameters obtained using CP2K and BLYP-D2/DZVP. Wet surface (containing the single physisorbed water monolayer): (a) top view (silanol top layer only shown) and (b) side view.

Table S1: Theory level validation: Geometric parameters of the dry α-quartz system obtained with various DFT functionals and basis sets[a]

Quantity	Description	BLYP/DZVP	BLYP-D2/DZVP	BLYP/TZV2P	BLYP-D2/TZV2P	PBE/TZV2P	PW91	Expt
			Geometric parameters: top view (see Figure S2(a))					
r_{Si-OH}	SI, internal bond	1.68	1.68	1.66	1.66	1.66		
r_{Si-OH}	SII, internal bond	1.67	1.67	1.64	1.65	1.64		
θ_{O-Si-O}	SII-SI, internal, angle	109.85	111.08	109.21	110.22	109.57		
r_{SiO-H}	SI, internal bond	1.00	1.00	0.99	0.99	0.99		
r_{SiO-H}	SII, internal bond	1.00	1.00	0.99	0.99	0.99		
θ_{Si-O-H}	SI, internal, angle	111.82	111.88	113.20	113.18	112.14		
θ_{Si-O-H}	SII, internal, angle	113.27	112.40	114.49	114.16	114.28		
$r_{SiOH-OSi}$	SII-SI, strong h-bond	1.79	1.78	1.80	1.81	1.78	1.74[b]	
$r_{SiOH-OSi}$	SI-SII, weak h-bond	2.03	2.03	2.08	2.08	2.10	2.11[b]	
θ_{H-O-Si}	SII-SI, strong h-bond, angle	132.09	132.69	133.72	133.99	133.72		
θ_{O-H-O}	SI-SII, weak h-bond, angle	169.18	170.51	167.93	169.04	168.95	168[b]	
θ_{H-O-H}	SI-SII, weak h-bond, angle	111.92	111.18	109.91	109.09	110.62		
r_{O-O}	silanol O - silanol O, distance 1		2.76			2.71	2.72[b]	
r_{O-O}	silanol O - silanol O, distance 2		2.78			2.77	2.73[b]	
r_{O-O}	silanol O - silanol O, distance 3		3.02			3.08	3.09[b]	
			Geometric parameters: side view (see Figure S2(b))					
r_{Si-O}	α-quartz, internal bond	1.66	1.66	1.64	1.64	1.64		1.61[c]
θ_{O-Si-O}	α-quartz, internal, angle	107.28	108.18	108.02	108.69	108.55		109[c,d]
$\theta_{Si-O-Si}$	α-quartz, internal, angle	140.76	138.24	143.50	140.55	142.25		144[c]

[a] All geometry optimizations were performed with CP2K and the indicated DFT functional and basis set. Bond lengths and bond angles are in Å and degrees, respectively. SI and SII refer to the two populations of silanols SiOH on which in the wet system are adsorbed the two populations of water molecules WI and WII, respectively.
[b] Calculation with VASP and PW91 (with a plane-wave basis set; calculation converged with regard to a *k*-point expansion), ref. [2]
[c] Experimental values are listed in ref. [9]
[d] The median value of the measured angle is 109°. The four measured values [9] are 108.57°, 108.72°, 108.97°, and 110.66°.

Table S2: Theory level validation: Geometric parameters and water molecule adsorption energy of the wet α-quartz system obtained with various DFT functionals and basis sets[a]

Quantity	Description	BLYP/DZVP	BLYP-D2/DZVP	BLYP/TZV2P	BLYP-D2/TZV2P	PBE/TZV2P	PW91
	Geometric parameters: top view (see Figure S3(a))						
r_{O-H1}	WI, internal bond	1.00	1.00	0.99	1.00	0.99	
r_{O-H1}	WII, internal bond	1.00	1.00	0.99	0.99	0.99	
$\theta_{H1-O-H2}$	WI, internal, angle	107.18	107.53	107.52	107.91	107.65	
r_{H1-O}	WI-WII, weak h-bond 3	1.82	1.81	1.83	1.82	1.82	
r_{H2-O}	WI-WII, weak h-bond 2	1.88	1.86	1.89	1.88	1.88	
r_{H1-O}	WII-WI, weak h-bond 1	1.92	1.94	1.92	1.93	1.94	
$\theta_{H2-O-H1}$	WI-WII, weak h-bond 3, angle	116.41	116.27	116.27	115.99	115.64	
θ_{O-H2-O}	WI-WII, weak h-bond 3, angle	163.14	164.55	163.91	165.24	164.55	
θ_{O-H1-O}	WI-WII, weak h-bond 2, angle	157.44	158.59	157.99	159.29	158.42	
$\theta_{H1-O-H2}$	WII-WI, weak h-bond 1, angle	119.59	119.11	120.06	120.30	120.57	
θ_{O-H1-O}	WII-WI, weak h-bond 1, angle	159.33	158.93	158.92	159.15	158.53	
r_{O-O}	silanol O - silanol O, distance 1		2.55			2.58	2.55[b,d]
r_{O-O}	silanol O - silanol O, distance 2		2.65			2.61	2.63[b,d]
r_{O-O}	silanol O - silanol O, distance 3		3.38			3.42	3.44[b,d]
r_{O-O}	silanol O - water O, distance 1		2.76			2.68	2.67[b,d]
r_{O-O}	silanol O - water O, distance 2		2.78			2.70	2.72[b,d]
r_{O-O}	water O - water O, distance 1		2.80			2.83	2.77[b,d]
r_{O-O}	water O - water O, distance 2		2.82			2.89	2.87[b,d]
	Geometric parameters: side view (see Figure S3(b))						
r_{Si-O}	α-quartz, internal bond	1.66	1.66	1.64	1.64	1.64	
θ_{O-Si-O}	α-quartz, internal, angle	106.68	107.60	107.61	108.77	107.83	
$\theta_{Si-O-Si}$	α-quartz, internal, angle	141.45	138.94	144.20	140.68	143.59	
$\theta_{Si-O-Si}$	α-quartz, internal, angle	137.95	134.85	140.34	137.09	139.07	
r_{SiO-H}	SI, internal bond	1.02	1.03	1.00	1.01	1.01	
r_{O-H1}	WII, internal bond	1.00	1.00	0.99	0.99	0.99	
$\theta_{H1-O-H2}$	WII, internal, angle	101.82	102.04	102.67	102.72	102.32	
$r_{SiOH-OSi}$	SI-SII, strong h-bond 1	1.56	1.57	1.60	1.60	1.57	
r_{SiOH-O}	SI-WI, strong h-bond 2	1.69	1.63	1.75	1.69	1.67	
r_{H2-OSi}	WII-SII, strong h-bond 3	1.72	1.66	1.76	1.69	1.70	
r_{H2-O}	WI-WII, weak h-bond 2	1.88	1.86	1.89	1.87	1.88	
$\theta_{SiOH-O-H2}$	SI-WI, strong h-bond 2, angle	104.76	104.38	103.85	102.78	103.46	
$\theta_{H2-O-H2}$	WI-WII, weak h-bond 2, angle	89.72	89.97	89.92	90.57	89.39	
	Adsorption energy per H_2O in layer						
E_{ads}	Adsorption energy	-15.86	-20.34	-12.89	-17.27	-15.77	-15.0[b,d]
							-15.2[c,d]
	(Doubled surface)		(-20.60)				

[a] All geometry optimizations were performed with CP2K and the indicated DFT functional and basis set. Bond lengths and bond angles are in Å and degrees, respectively. The adsorption energy (per water molecule, in kcal/mol) $E_{ads} = (E_{total} - E_{surf} - nE_{H_2O})/n$, where E_{total} is the energy of the surface including a monolayer of water, E_{surf} is the energy for the optimized clean hydroxylated surface system, E_{H_2O} is the energy for an isolated water molecule, and n is the number of adsorbed water molecules. SI and SII refer to the two populations of silanols SiOH on which in the wet system are adsorbed the two populations of water molecules WI and WII, respectively.

[b] Calculation with VASP and PW91 (with a plane-wave basis set; calculation converged with regard to a k-point expansion), ref. [2]

[c] Calculation with VASP and PW91 (with a plane-wave basis set; calculation converged with regard to a k-point expansion), ref. [3]

[d] Note that the water adlayer computed in refs. [2,3] is slightly different, differing by an overall rotation of 120° relative to the one computed by us. Nevertheless, the various O-O separation distances and adsorption energies are nearly identical, justifying our comparison with the results obtained in refs. [2,3]

Table S3: Summary of Trajectories 1–23[a] showing whether the first H_2SO_4 deprotonation occurred and if so, the conditions.[b]

Trajectory	Basis	System	Temperature [K]			Duration	H_2SO_4 donates/accepts H-bonds			Deprotonation?					Comments
			T_0	T_{avg}	ΔT	[ps]	donates (to)	accepts	sum		time t [ps]	to	HSO_4^- H-bonds	further PT?	
1	DZVP	Small	250	266	+16	10.00	1 (WII)	3	4	Y	0.92	WII	4	Y	
2	DZVP	Small	250	264	+14	5.00	2 (WI, WI)	2	4	N	na	na	na	na	H_2SO_4 is a double H-bond donor.
3	TZV2P	Small	250	259	+9	6.55	1 (WI)	3	4	Y	2.19	WI	4	maybe	Dissociates briefly at 0.87 ps.
4	TZV2P	Small	250	258	+8	9.61	1 (WI)	0	1	N	na	na	na	na	Insufficient solvation.
5	DZVP	Large	250	257	+7	6.37	1 (WI)	4	5	Y	0.49	WI	5	Y	
6	DZVP	Large	250	256	+6	5.08	1 (WI)	0	1	N	na	na	na	na	Insufficient solvation.
7	DZVP	Small	250	268	+18	5.00	2 (WI, WII)	0	0	N	na	na	na	na	H_2SO_4 is a double H-bond donor.
8	DZVP	Small	250	263	+13	5.00	1 (WII)	2	3	Y	0.39	WII	3	Y	
9	DZVP	Small	250	259	+9	5.00	1 (WII)	3	4	Y	0.58	WII	4	Y	
10	DZVP	Small	250	260	+10	5.00	1 (WII)	3	4	Y	0.72	WII	4	Y	
11	DZVP	Small	250	257	+7	5.00	1 (WII)	1	2	N	na	na	na	na	Insufficient solvation.
12	DZVP	Small	250	271	+21	5.00	2 (WI, WII)	2	4	N	na	na	na	na	H_2SO_4 is double H-bond donor.
13	DZVP	Small	250	270	+20	5.00	1 (WII)	2	3	Y	1.02	WII	3	Y	
14	DZVP	Small	250	269	+19	5.00	1 (WII)	4	5	Y	0.54	WII	5	Y	
15	DZVP	Small	250	266	+16	5.00	1 (WI)	2	3	Y	4.63	WI	3	N	Dissociates late; reforms neutral within 0.3 ps; thus no further PT.
16	DZVP	Small	250	264	+14	5.00	2 (WII, WII)	2	4	Y	0.58	WII	4	Y	Proton wire leads to reformation of neutral within 0.3 ps.
17	DZVP	Small	250	267	+17	5.00	1 (WI)	3	4	Y	0.38	WI	4	Y	
mean				263	+13						1.1				
18	DZVP	Small	273	280	+10	5.00	1 (WII)	4	5	Y	0.58	WII	5	Y	Reforms neutral and dissociates again at 1.26 ps.
19	DZVP	Small	273	290	+17	5.00	2 (WI, WII)	2	4	N	na	na	na	na	H_2SO_4 is a double H-bond donor.
20	DZVP	Small	300	325	+25	10.00	1 (WII)	4	5	Y	0.58	WII	5	Y	
21	DZVP	Small	300	318	+18	5.00	2 (WI, WI)	2	4	N	na	na	na	na	H_2SO_4 is a double H-bond donor.
22	DZVP	Small	330	337	+25	5.00	1 (WI)	3	4	Y	0.47	WI	4	Y	
23	DZVP	Small	330	342	+18	5.00	2 (WI, WII)	2	4	N	na	na	na	na	H_2SO_4 is a double H-bond donor.

[a] Our 24th trajectory, Trajectory 5a, is not shown here since it describes a second deprotonation event. It is the continuation of Trajectory 5 after addition of a second water layer on top of HSO_4^- on wet quartz present at time of 6.37 ps in Trajectory 5. The duration of Trajectory 5a was 1.92 ps.

[b] All calculations in the *NVE* ensemble employed CP2K and BLYP-D2 with the DZVP or TZV2P basis set, a time step of 0.4 fs, and proceeded from an equilibrated simulation with the identical basis set in the *NVT* ensemble at the target temperature. The H-bonding environment of H_2SO_4 and HSO_4^- is also shown. Y = yes, N = no, na = not applicable, PT = proton transport.

(a) t = 0.00 ps:
H_2SO_4 released 3.5 Å above the wet quartz surface

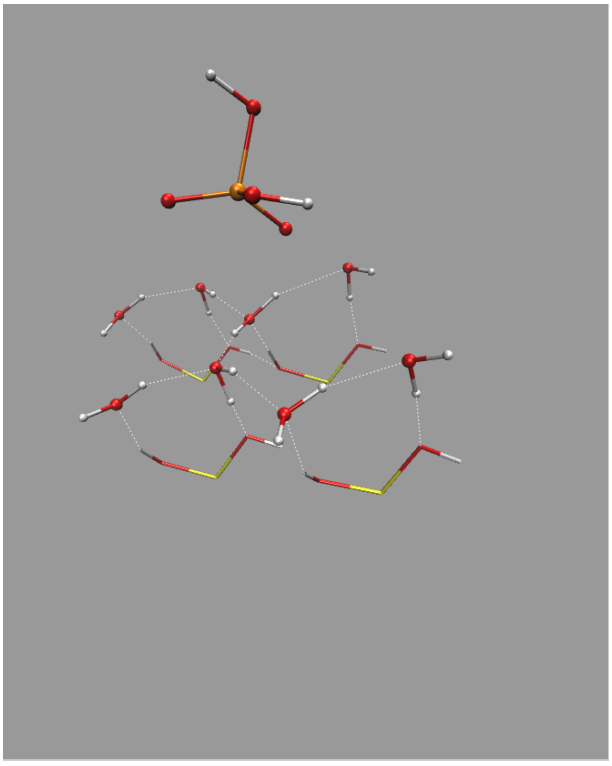

(c) t = 0.67 ps:
Contact Ion Pair $HSO_4^- \cdots H_3O^+$

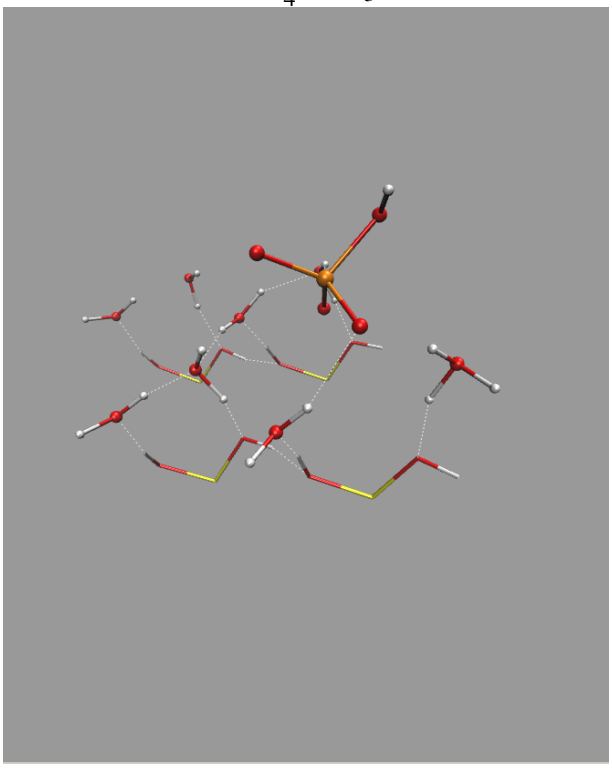

(b) t = 0.54 ps:
$H_2O \cdots H_2SO_4$ H-bond

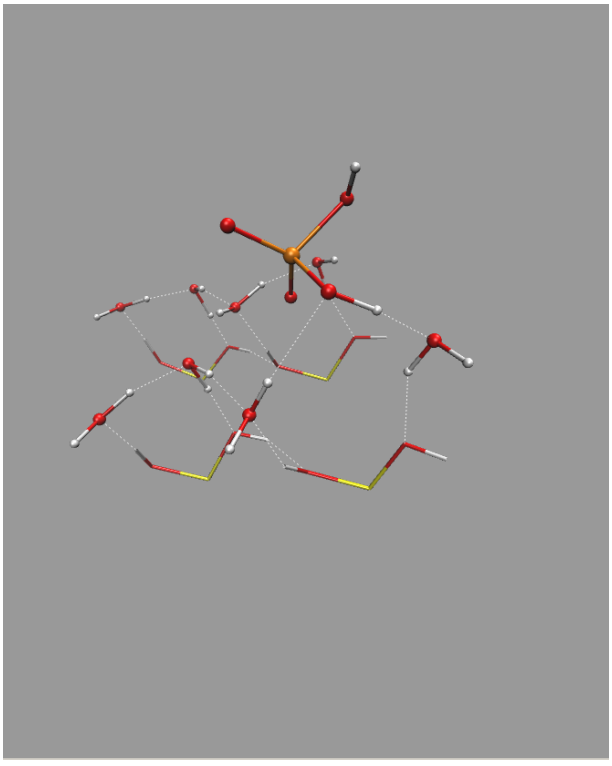

(d) t = 1.64 ps:
Solvent-Separated Ion Pair $HSO_4^- \cdots H_2O \cdots H_3O^+$

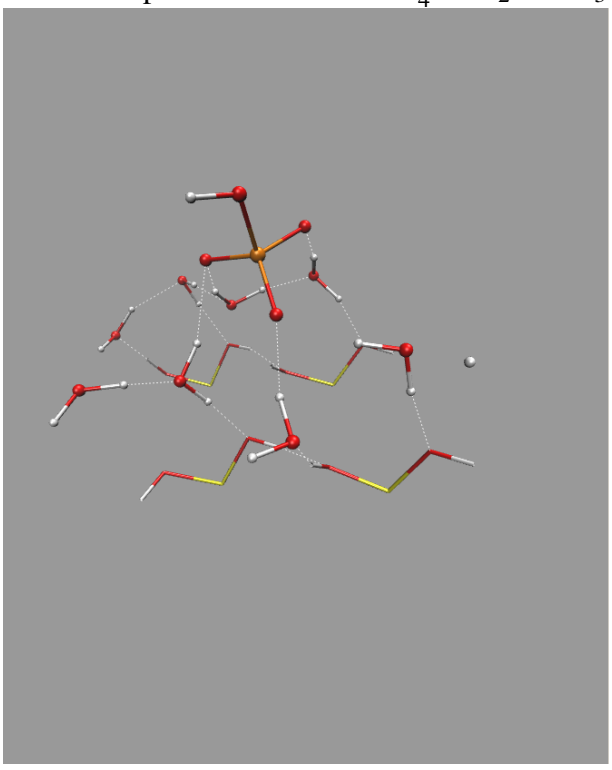

Figure S4: Snapshots showing the H_2SO_4 first deprotonation and subsequent proton migration at 300 K (perspective view; silanol top layer only shown; sulfur, orange; oxygen, red; hydrogen, white; silicon, yellow). In panel (d) the water molecule to which H^+ has transferred is located across the periodic boundary of the simulation cell, at the left side of the image. The data are from Trajectory 20.

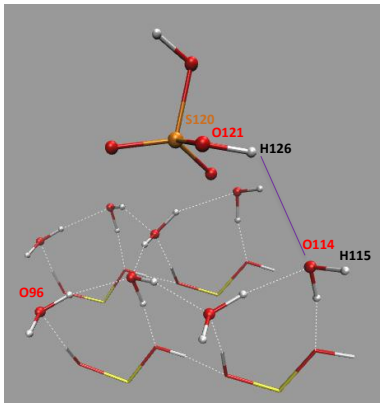

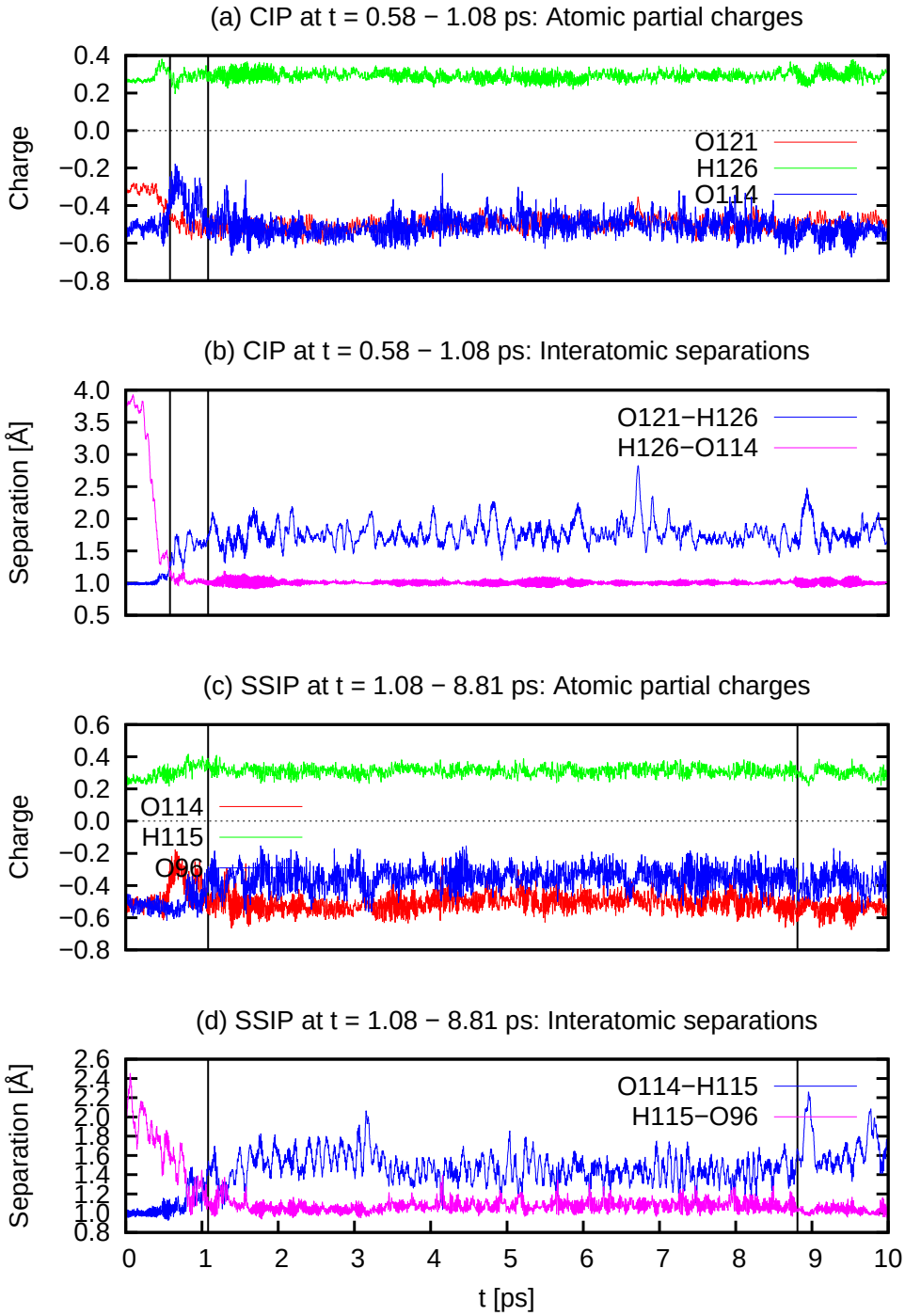

Figure S5: Interatomic separations and partial Mulliken charges of relevant atoms during the proton migration at 300 K. The snapshot (at t = 0.00 ps) shows the atom labels. The black vertical lines draw attention to relevant time intervals. The data are from Trajectory 20. See also Figure S4(a)–(d) for geometries.

(a) t = 0.56 ps:

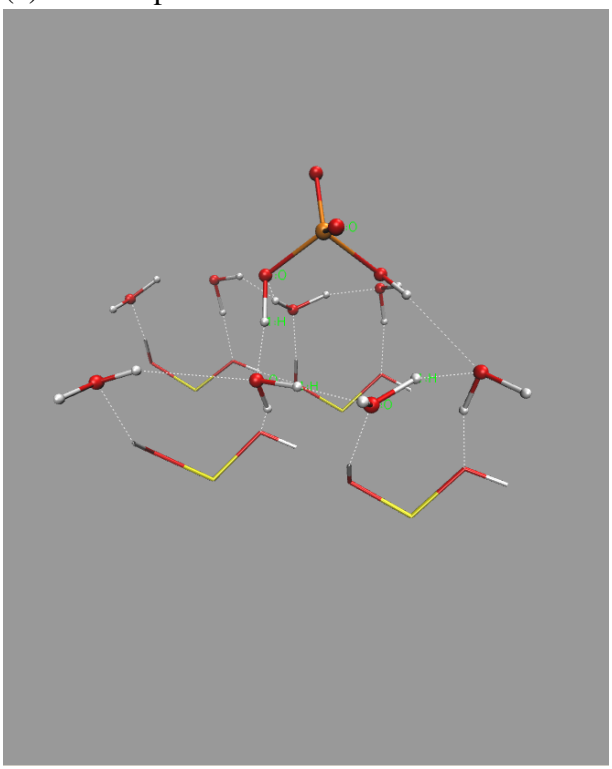

(c) t = 0.86 ps:

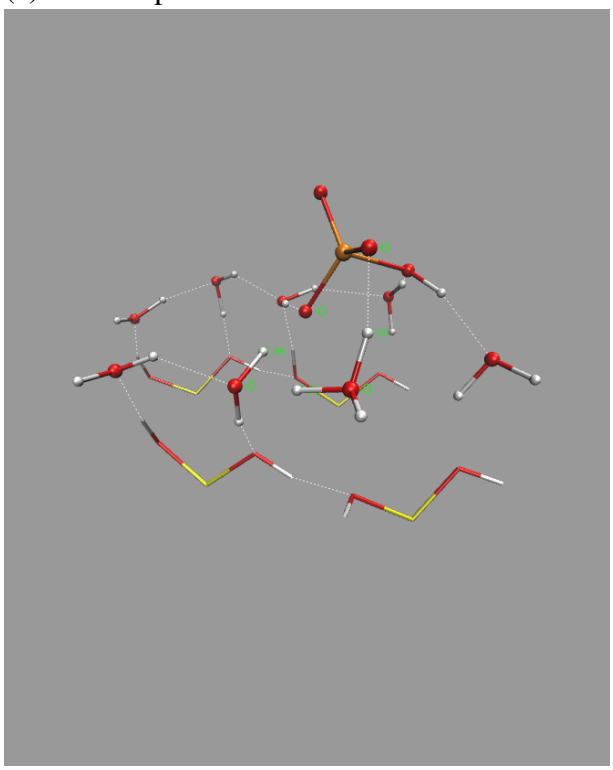

(b) t = 0.59 ps:

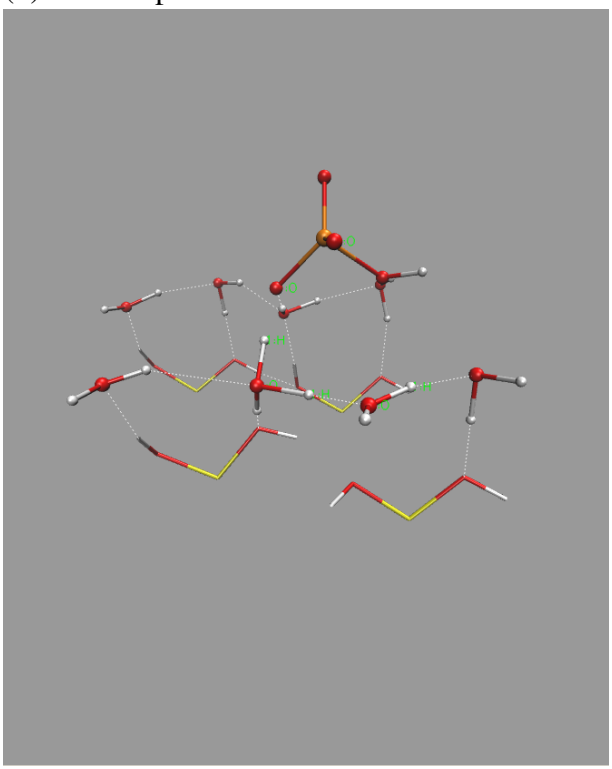

(d) t = 0.91 ps:

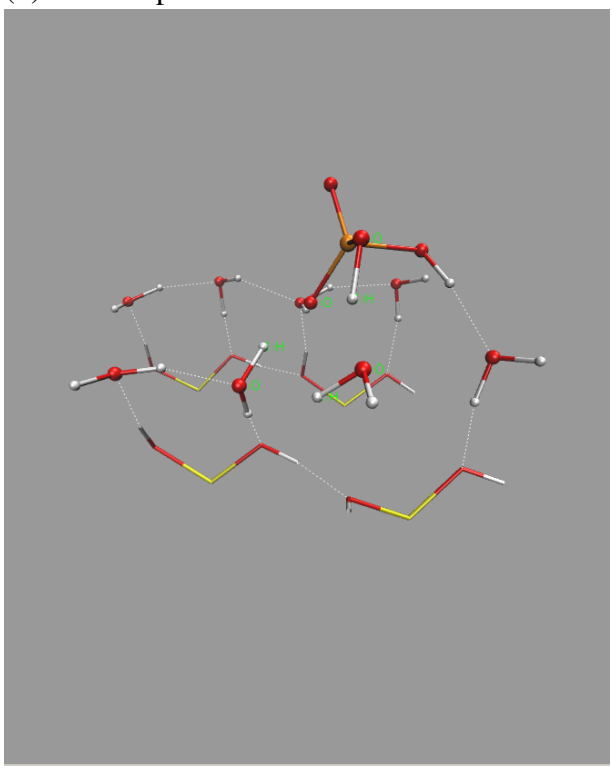

Figure S6: Snapshots from Trajectory 16 (250 K) showing waters acting as a proton wire to reform neutral H_2SO_4 with the proton on a different H_2SO_4 oxygen (perspective view; silanol top layer only shown).

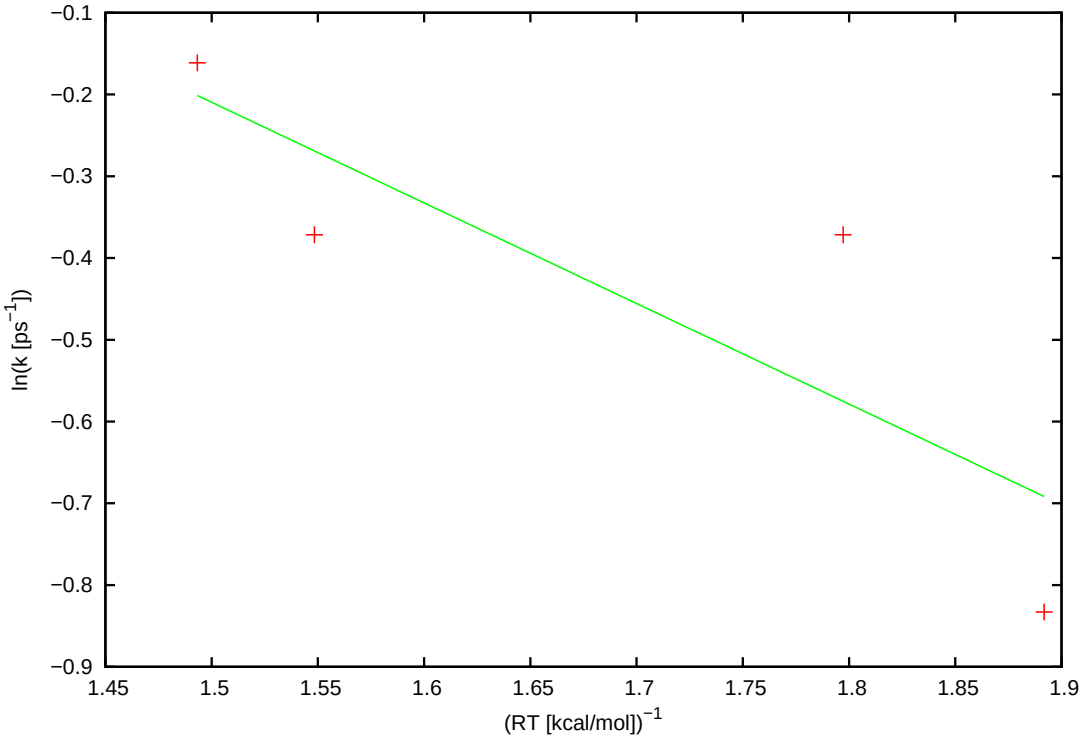

Figure S7: Arrhenius plot for the rate $k = 1/t_{\text{avg}}$ of the first deprotonation of H_2SO_4 on wet quartz as a function of temperature.

(a) g_{OO} within the water layer (250 K)

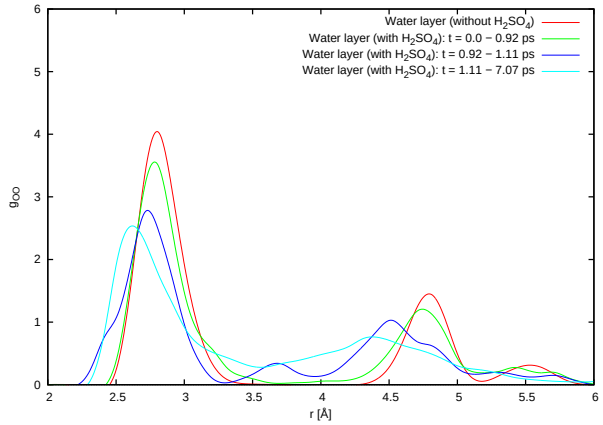

(b) g_{OO} of bulk ice (250 K) and bulk water (300 K)

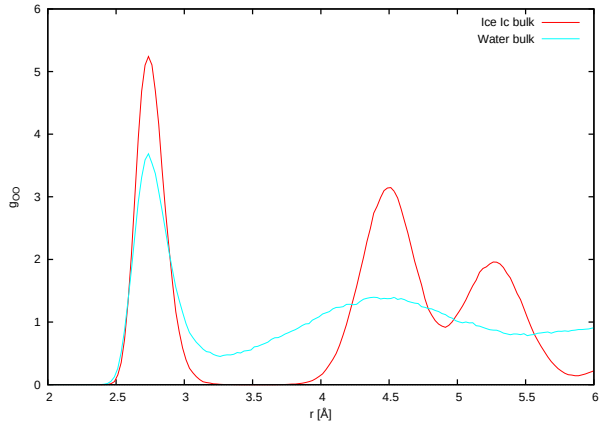

(c) g_{OH} within the water layer (250 K)

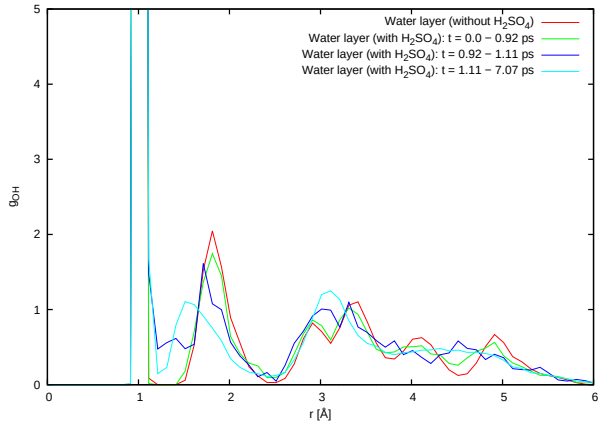

(d) g_{OH} of bulk ice (250 K) and bulk water (300 K)

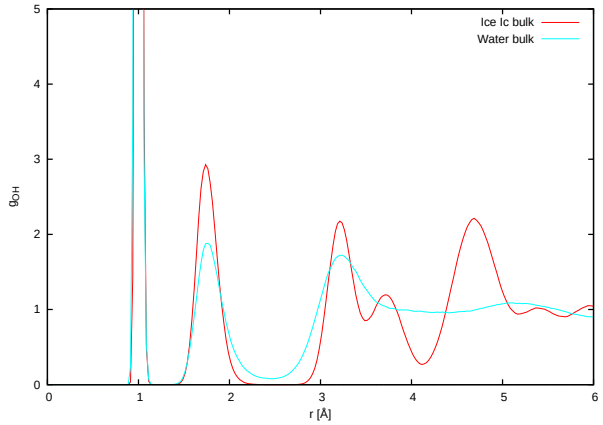

Figure S8: Radial distribution functions within the water adlayer obtained over the indicated time intervals during the proton migration at 250 K (Trajectory 1) compared with those of neat bulk ice (250 K) and bulk water (300 K). The progressive disordering with time is visible.

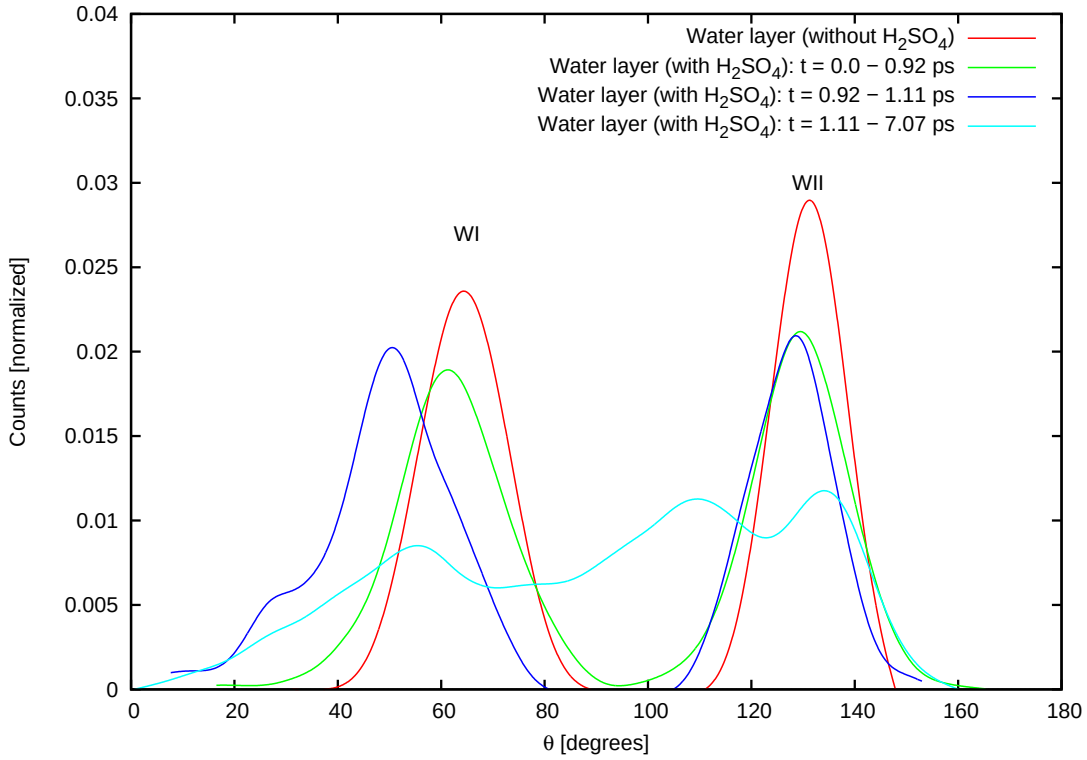

Figure S9: Distributions of molecular orientations θ within the water adlayer obtained over the indicated time intervals during the proton migration at 250 K (Trajectory 1). The progressive disordering with time is visible. WI (in-plane waters) and WII (H-down waters) are the two populations of water molecules. θ is the angle between the water H-O-H bisector and the surface normal.

(a) t = 0.00 ps: Before introduction of H_2SO_4 to the surface
(separate 5 ps trajectories)

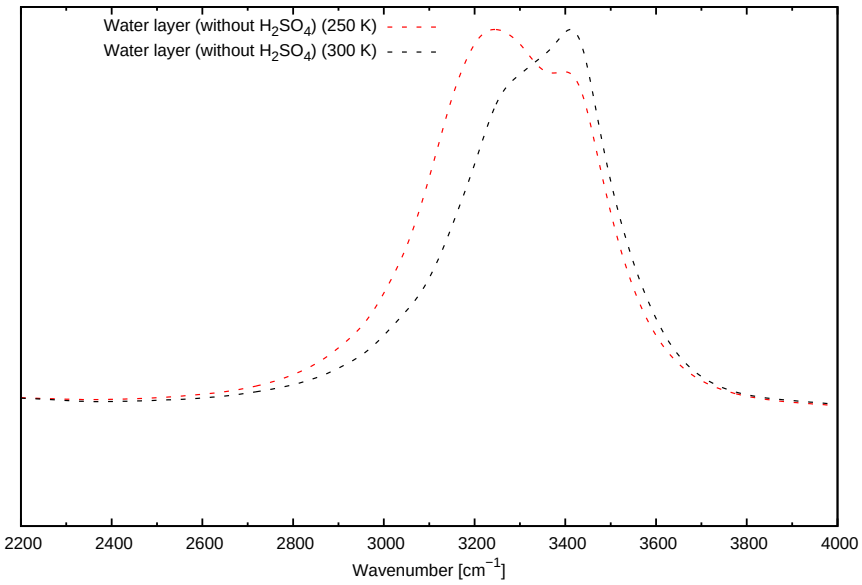

(b) t = 1.11–7.07 ps (250 K) and 1.08–8.81 ps (300 K): After introduction of H_2SO_4
(existence of SSIP $HSO_4^- \cdots H_2O \cdots H_3O^+$)

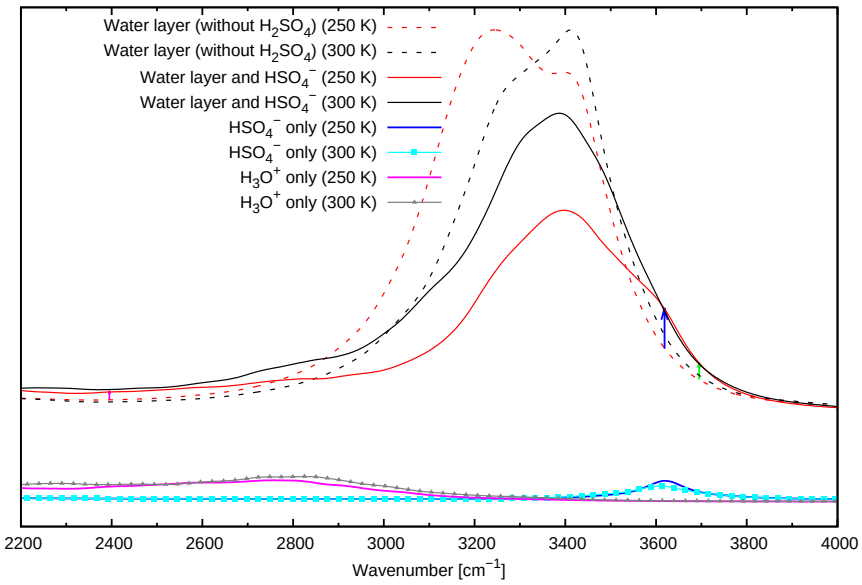

Figure S10: Comparison of vibrational spectra (VDOS) during the proton migration at 250 and 300 K. VDOS were computed for the indicated time interval. In panel (b) (red curve), HSO_4^- causes the weak shoulder at about 3620 cm^{-1} (free water OH also contributes in this region), and H_3O^+ causes the small increase in intensity in the broad region at 2800 cm^{-1} and below. The data are from Trajectory 1 (250 K) and Trajectory 18 (300 K). See also Figure S4(a) and Figure S4(d) for the geometries corresponding to the 300 K spectra in panels (a) and (b), respectively. They can be compared to the very similar structures at 250 K in Figure 3(a) and Figure 3(d) in the main text.

Table S4: Relative and interaction energies (all in kcal/mol) and characteristics of some minimum energy structures of neutral and deprotonated H_2SO_4 on the wet quartz surface.[a]

Structure name[b]	Encountered in Trajectory	H_2SO_4 donates/accepts H-bonds			E_{rel}	E_{int}	Comments
		donates (to)	accepts	sum			
c-a	7	2 (WI, WII)	2	4	0.0 (0.0)	-29.5 (-23.8)	Neutral (*cis*).
c-b	2	1 (WI)	1	2	0.7	-28.9	Neutral (other non-*trans* rotamer).
c-c	12	2 (WII, WII)	2	4	7.0	-22.6	Neutral (other non-*trans* rotamer).
c-d	16	2 (WII, WII)	1	3	8.6	-20.9	Neutral (other non-*trans* rotamer).
n-a	11	1 (WII)	2	3	5.9	-23.7	Neutral (*trans*).
n-b	1	1 (WII)	1	2	9.6 (8.7)	-20.0 (-15.2)	Neutral (*trans*).
n-c	8	1 (WII)	1	2	9.7	-19.8	Neutral (*trans*).
n-d	9	1 (WII)	2	3	13.3	-16.2	Neutral (*trans*).
i-a	1	na	na	na	6.3 (6.2)	-23.3 (-17.7)	Ionized (SSIP).
i-b	13	na	na	na	7.9	-21.7	Ionized (SSIP).
i-c	17	1 (WI)	3	4	8.2	-21.4	Ionized (CIP).
i-d	1	1 (WII)	2	3	12.3 (11.3)	-17.2 (-12.5)	Ionized (CIP).

[a] E_{rel} are relative energies with respect to the lowest energy configuration, the neutral *cis* c-a structure. Interaction energies $E_{int} = E$(configuration) - E(isolated wet quartz surface) - E(isolated H_2SO_4 molecule) (no correction for basis set superposition error). The starting points for these 0 K energy minimizations were some points in Trajectories 1–17 (excluding Trajectories 5 and 6) from Table S3. The H-bonding environment of H_2SO_4 and HSO_4^- is also shown as in Table S3. Calculations used the small system and CP2K with BLYP-D2 and the DZVP basis set. Some TZV2P basis set results are shown in parentheses; using the larger basis set does not change the geometries or the energy ordering of configurations. See also Figure S11, Figure S12, and Figure S13 for the c (neutral *cis*), n (neutral *trans*), and i (singly ionized, SSIP or CIP) configurations, respectively.

[b] The structure name *x*-*y* follows the convention used in the Re et al. study[5] of $H_2SO_4 \cdots (H_2O)_{n=1-5}$ clusters, where the configuration type *x* = n (neutral, *trans* isomer of H_2SO_4), c (neutral, *cis* or one of the other two non-*trans* rotamers of H_2SO_4, see ref. [4]), i (singly ionized/deprotonated H_2SO_4, i.e., bisulfate HSO_4^-), ii (doubly ionized/deprotonated H_2SO_4, i.e., sulfate SO_4^{2-}, not observed in the smaller system); and the label *y* = a, b, c, $\cdots$ labels each configuration type in order of increasing energy.

c-a: 0.0 kcal/mol

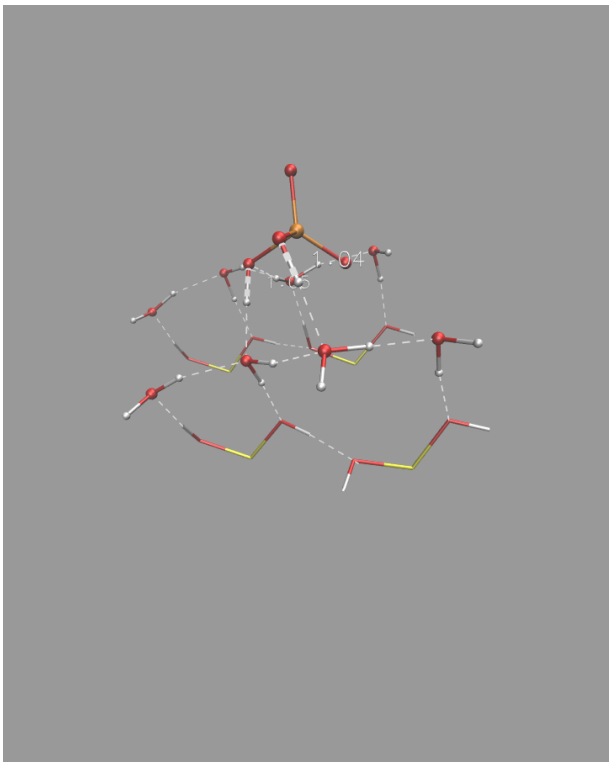

c-c: 7.0 kcal/mol

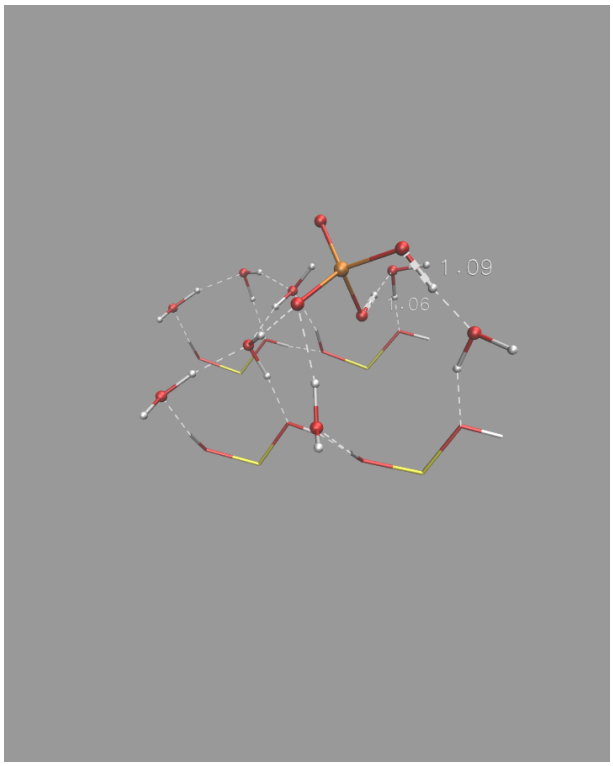

c-b: 0.7 kcal/mol

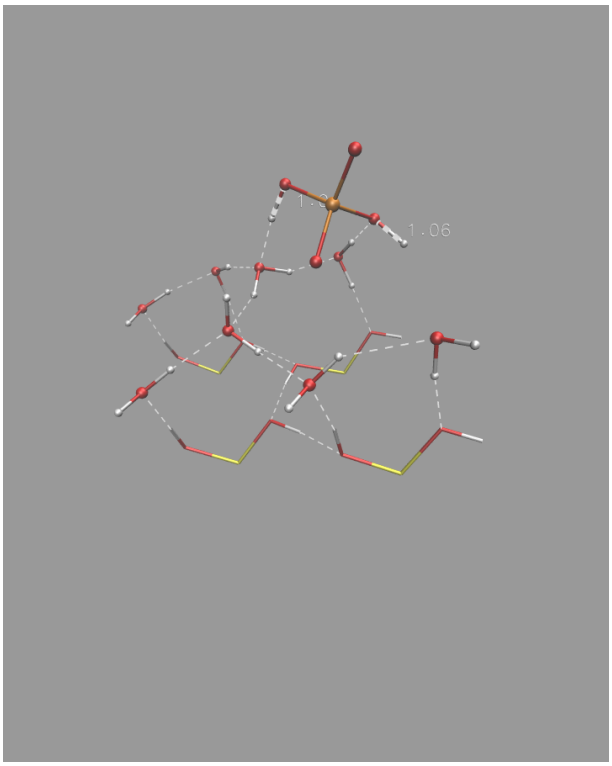

c-d: 8.6 kcal/mol

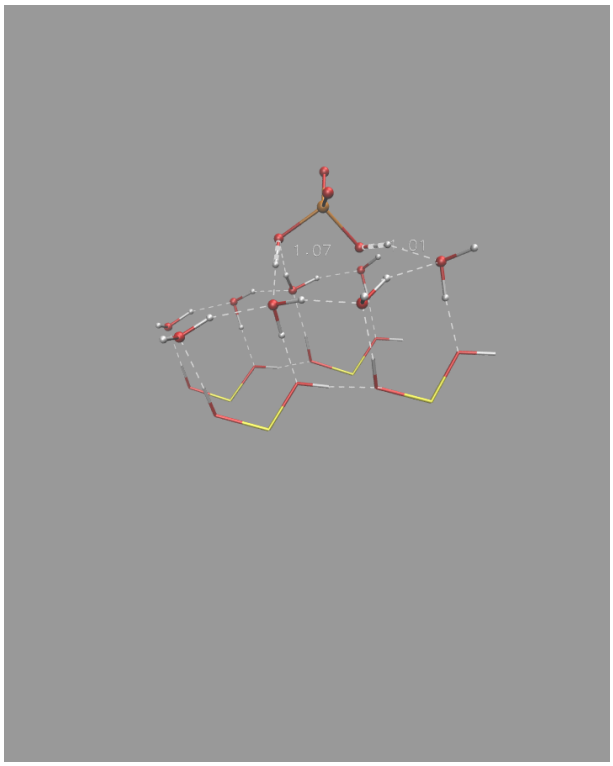

Figure S11: Some geometry-optimized c (neutral *cis*) configurations and their relative energies (calculated with the DZVP basis set; perspective view; silanol top layer only shown). Only the top portion of the quartz slab is shown. See Table S4 for details.

n-a: 5.9 kcal/mol

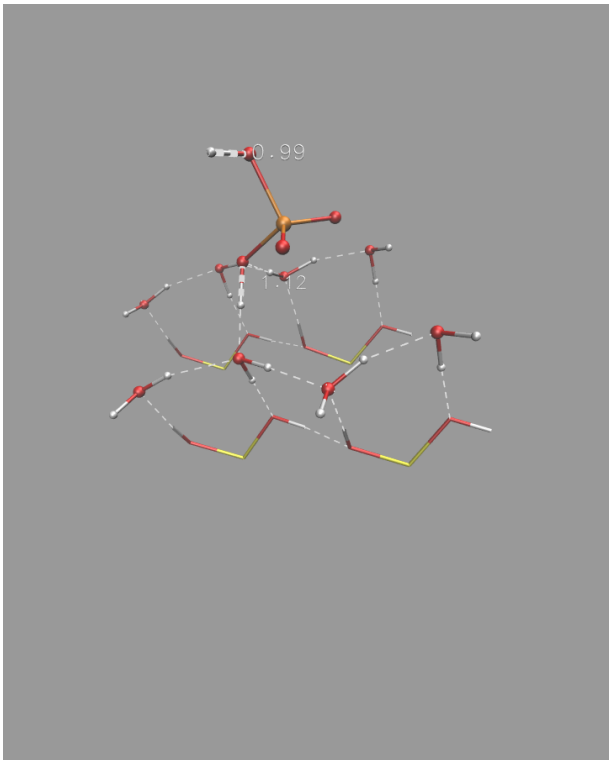

n-c: 9.7 kcal/mol

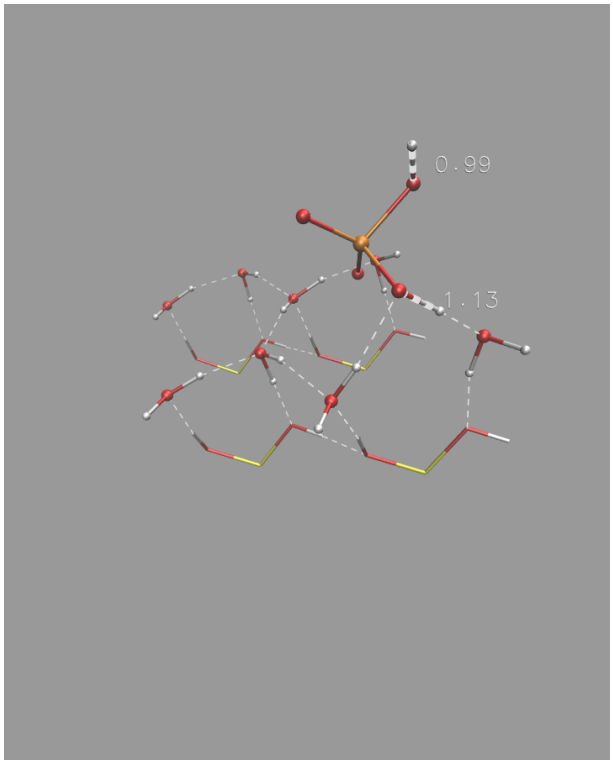

n-b: 9.6 kcal/mol

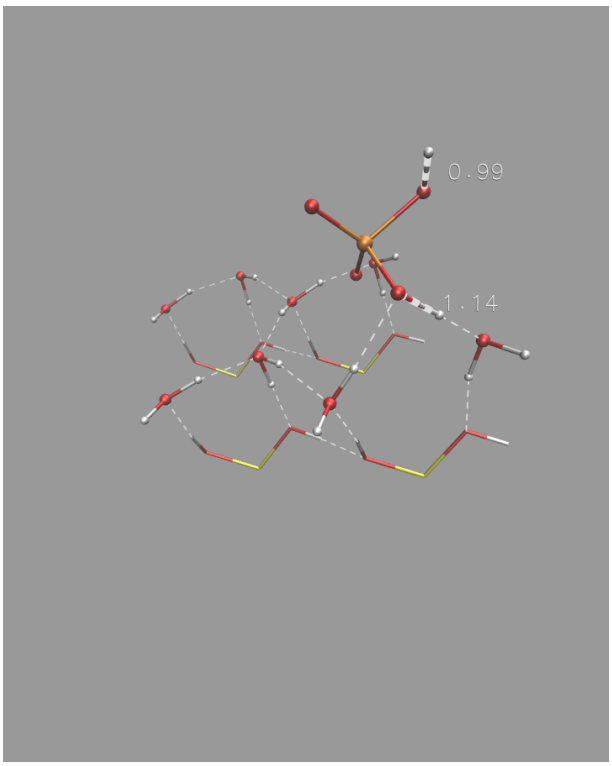

n-d: 13.3 kcal/mol

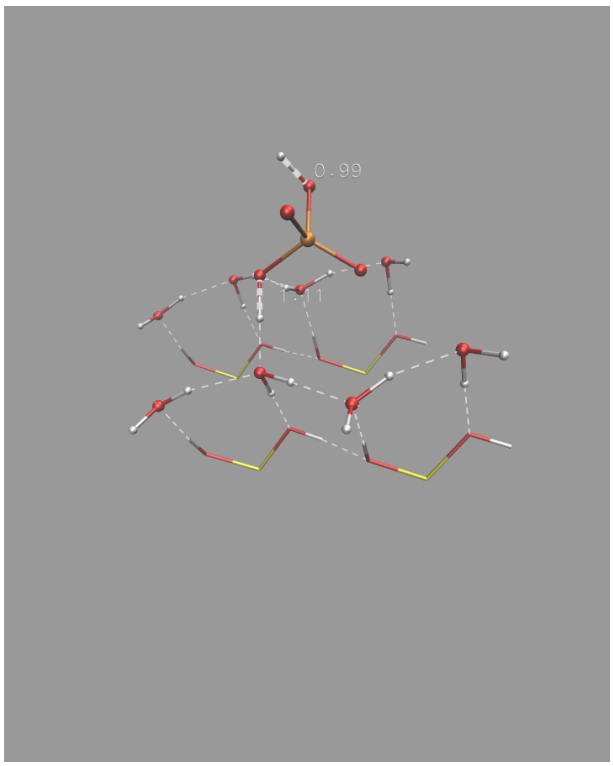

Figure S12: The n (neutral *trans*) configurations. See caption to Figure S11.

i-a: 6.3 kcal/mol (SSIP)

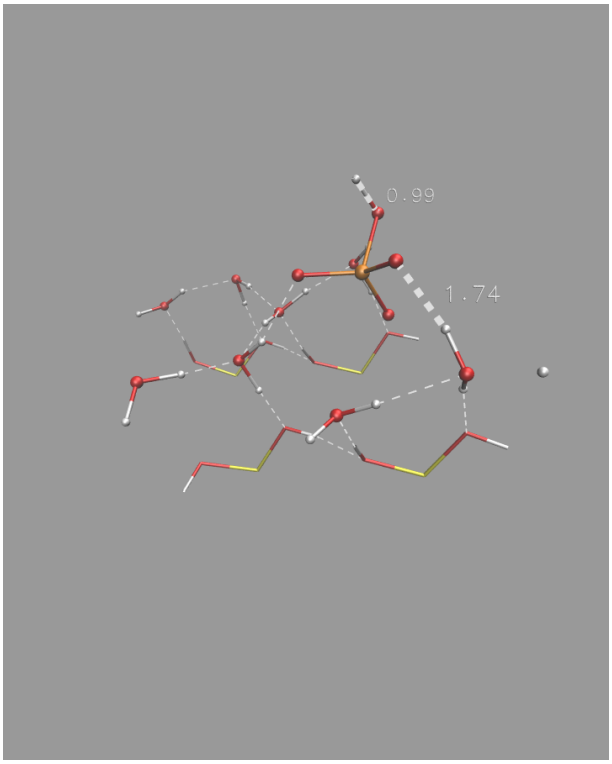

i-c: 8.2 kcal/mol (CIP)

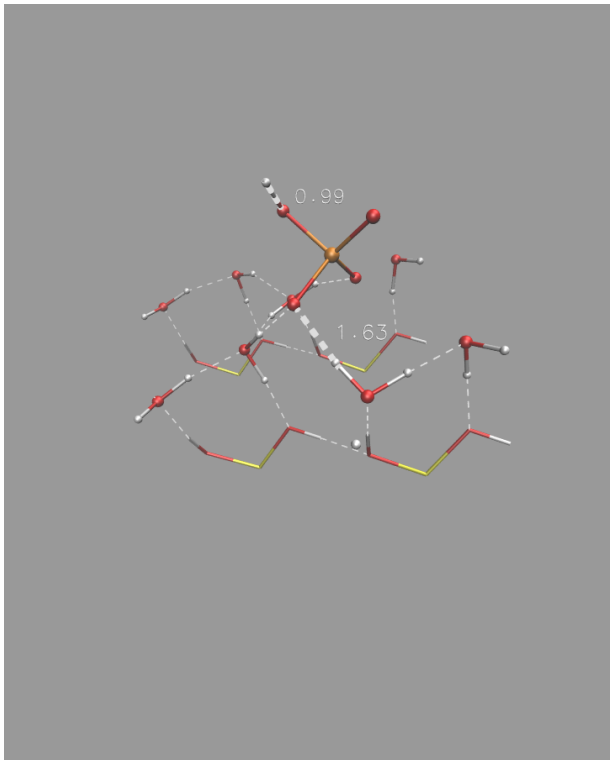

i-b: 7.9 kcal/mol (SSIP)

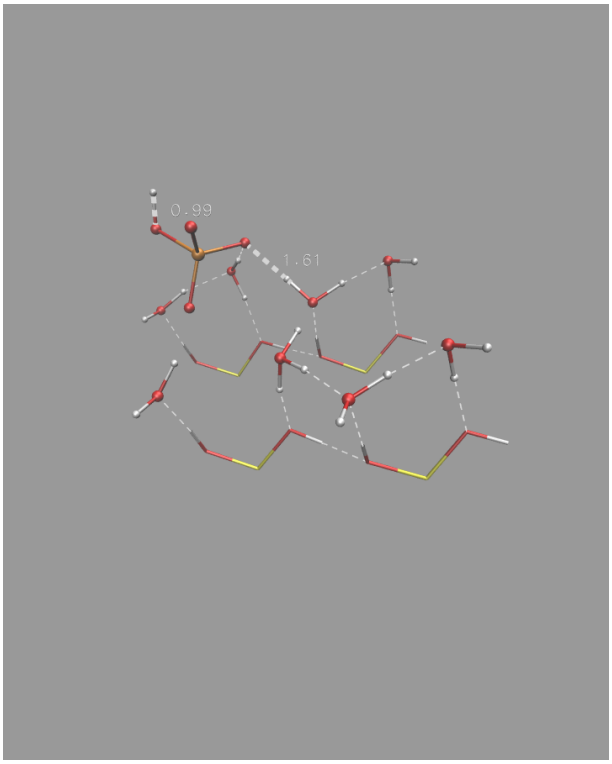

i-d: 12.3 kcal/mol (CIP)

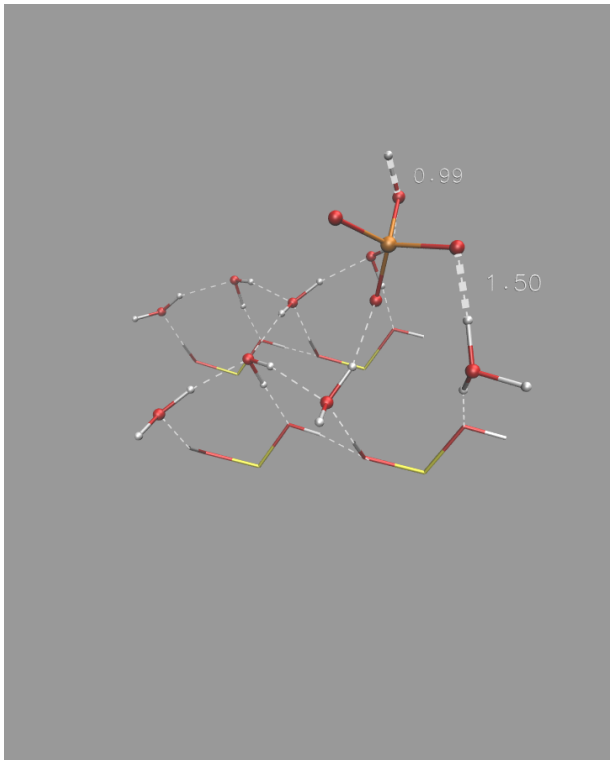

Figure S13: The i (singly ionized, SSIP or CIP) configurations. See caption to Figure S11.